INSTITUTO NACIONAL DE METEOROLOGIA

SUB. GRAL. DE PROGRAMAS ESPECIALES E INVESTIGACION CLIMATOLOGICA

ATMOSPHERIC RESPONSE TO A CO_2 DOUBLING OF THE ARPEGE CLIMATE MODEL OVER EUROPE

Maria Jesús Casado
Asunción Pastor

SERVICIO DE ANALISIS
E INVESTIGACION DEL CLIMA

INFORME Nº 10

OCTUBRE
1996

ATMOSPHERIC RESPONSE TO A CO_2 DOUBLING OF THE ARPEGE CLIMATE MODEL OVER EUROPE

Maria Jesús Casado, Asunción Pastor

SAIC / Instituto Nacional de Meteorologia
Madrid, Spain

October, 1996

Contents

Abstract

In this paper we analyze a regional climate change scenario over Europe induced by doubling of carbon dioxide concentration, simulated by the atmospheric climate global circulation model (GCM) ARPEGE, developed at Météo-France. This model has high vertical resolution in the stratosphere and predicts the evolution of the ozone mixing ratio. The version we use runs with a varible resolution (T63s), varying from T200 over Europe to T21 over the southern Pacific. Two five-year simulations are carried out (the control and the perturbed runs). The perturbed run is performed using SST and sea-ice extents obtained from a scenario simulation by the Max Planck Institute. We focus our study on the seasonal anomalies in winter (what we call DJF) and in summer (JJA), also we analyze the annual cycle. We divide our domain (Europe) in four boxes (NW, NE, SW and SE). The model predicts a warming in the troposhere not as large as in most previous models and a decrease of precipitation while other studies obtained an increase.

1 Introduction

The atmospheric concentrations of carbon dioxide and other radiative trace gases have been increasing as a result of energy generation, transportation, and industrial, agricultural and other human activities since the beginning of the last century (Report of the DOE Multi-Laboratory Climate Change Committee, 1990 [9]). These increases will enhance the greenhouse effect through their absorption of thermal infrared radiation resulting on average in an additional warming of the Earth's surface (IPCC,1990,1992 [17] [18]). But as this warming is not expected to be uniform along a latitude circle, it is crucial of assessing impacts at regional scale; because it is at this scale, 100 km or finer, where man-made activities represent the strongest environmental forcings. Various techniques are currently employed: a) statistical methods and b) dynamical regional high resolution models: 1) nested in global models and 2) a variable horizontal grid, with the higher resolution over a specific area of interest.

In the one-way nesting technique the meteorological initial and lateral boundary conditions necessary to drive the nested limited area model (LAM) over regions of interest are provided by the output of a GCM. This one-way nesting technique has been applied to climate simulation (Giorgi 1990 [13]) and has the advantage that any subdomain and any grid size may be obtained, but the inconvenience is the contamination of the local climate by systematic errors in the large scale which also exists with variable resolution models. The other possibility uses a global model with variable horizontal resolution. It has been used with grid point or finite elements models (Staniforth and Mitchell 1978 [29]) having high resolution over the area of interest and lower resolution outside, but being able to resolve synoptic waves. To study the impact of a CO_2 doubling on the European climate, we applied this latter approach. The method we used here (Courtier and Geleyn 1988 [5]) employs a spectral model and is based on the transformation introduced by Schmidt

(1977 [28]) a conformal mapping is defined between the Earth and another sphere, being the equations discretised on the latter: the grid spacing decreases monotically in both directions when going from one pole to another pole of the sphere. This method has the same flexibility as the nesting approach as far as the choice of the domain and the resolution are concerned. But it may be computationally more expensive than the nesting technique and moreover the resolution may be strongly varying with space (Déqué and Piedelievre 1995 [8]). Following Mahfouf et al. (1994 [22]) and Déqué and Piedelievre (1995 [8]), an alternative method to ocean coupling has been applied. At the lower boundary of the atmospheric GCM, sea surface temperatures (SST) are specified. As no ocean coupling is needed, the costs of computation are considerably reduced and since, the atmosphere equilibrates in a few months with the prescribed SST besides the use of an atmospheric model that has a higher resolution and more detailed parametrizations.

The present study is organized as follows. In section 2 we briefly review the experiments design. In section 3 a brief description of the numerical model used for the experiments is given. Section 4 reviews the control simulation, showing the ability of the model to reproduce the observed climatology. In section 5 we discuss the European climate change scenario and finally in section 6 we summarize our main conclusions and compare our results with the obtained by other authors.

2 Description of the experiments

Two sets of 5 years experiments with the stretched version of the ARPEGE climate model have been carried out: the control simulation uses the 10 year averages of the Atmospheric Model Intercomparison Project (AMIP) SST and a CO_2 concentration of 345 ppmv while the perturbed run has a CO_2 concentration of 690 ppmv and monthly anomalies were added to the SST. These SST anomalies result from a scenario simulation by

the Max Plank Institute (MPI) with a coupled ocean model, ECHAM1, for the atmosphere and LSG for the ocean (Cubasch et al. 1992 [6]). The SST anomalies were calculated between the control and the transient perturbed runs where the concentration of CO_2 increased by the rate of 1% by year. They are averaged over ten years (2056-2065) corresponding to the doubling CO_2 period according to IPCC scenario A. Over continents to be coherent with the ocean, the anomalies of the soil surface temperature between the control and the perturbed run at MPI have been added to the deep soil relaxation temperature. We have run these two simulations, and obtained the corresponding anomalies. We focus this study on the analysis of the atmospheric response for a doubling CO_2 experiment over Europe. The domain we consider is 35°N -70°N; 14.0°W-33°E, maritime grid points are excluded because we are mainly interested in the anomalies over land. We divide the domain into four subdomains, using the 50° N parallel and the 18° E meridian, obtaining the boxes: NW (British Isles, Benelux countries, northern and central Germany, Denmark, Norway and Sweden), NE (eastern Sweden, Finland, Poland, Baltic countries and western Russia), SW (Iberian peninsula, France, Italy, Switzerland, Austria, Croatia and Slovakia) and SE (Albania, Greece, Balkan countries, eastern Hungary, southern Poland and western Anatolia). Figure 1 shows these subdomains and the stretched T63 orography.

3 Model Description

The atmospheric GCM used in this paper is the climatic version of the ARPEGE/IFS forecast model developed by Météo-France and the European Centre for Medium-Range Weather Forecast (ECMWF), described by Déqué et al. (1994 [7]). It is based on its version 11c. The model is spectral with a variable resolution over the whole globe (Courtier and Geleyn 1988 [5]) and has its pole located in the Tyrrhenian Sea (40°N,12°E).

The truncation is T63 and the stretching factor c=3.5.The grid size varies from 60 km at the pole of stretching to 700 km at the antipodes (Déqué and Piedelievre 1995 [8]). Using a mapping of the sphere, the only modifications concern the horizontal derivatives, which are multiplied by the mapping factor m. This factor varies as a function of the geographical latitude and longitude, it decreases from c at the pole of stretching down to 1/c at the antipodes. The model uses the spectral transform method in the horizontal based on the longitude (λ), the sine of the latitude (μ), and a hybrid coordinate (η) following the orography, described by Simmons and Burridge (1981 [27]).

3.1 *Dynamics*

The dynamics include the numerical techniques by means of which long scale atmospheric transports are resolved. The basic equations of the model are:

hydrostatic equation

$$\frac{\partial \phi}{\partial \eta} = \frac{-RT}{p} \frac{\partial p}{\partial \eta} \tag{1}$$

thermodynamic equation

$$\frac{dT}{dt} - k\frac{Tw}{p} = \frac{-g}{c_p}\frac{\partial \eta}{\partial p}\frac{\partial F_h}{\partial \eta} + D_h \tag{2}$$

moisture equation

$$\frac{dq}{dt} = -g\frac{\partial \eta}{\partial p}\frac{\partial F_q}{\partial \eta} + D_q \tag{3}$$

momentum equation

$$\frac{d\vec{v}}{dt} + 2\Omega\vec{v} + RT\nabla lnp + \nabla\phi = -g\frac{\partial \eta}{\partial p}\frac{\partial F_v}{\partial \eta} + D_v \tag{4}$$

continuity equation

$$\frac{\partial}{\partial \eta}(\frac{\partial p}{\partial t}) + \nabla.(\vec{v}\frac{\partial p}{\partial \eta}) + \frac{\partial}{\partial \eta}(\dot{\eta}\frac{\partial p}{\partial \eta}) = 0 \tag{5}$$

The atmosphere is assumed to be a mixture of dry air and water vapor,

two perfect gases. The latent heat of vaporization, and the saturated partial pressure of water vapor over liquid water are computed by the Clausius-Clapeyron relations. The atmospheric prognostic variables, the logarithm of surface pressure and the orography are represented by a truncated series of surface spherical harmonics.

$$X(\lambda,\mu,\eta,t) = \sum_{n=0}^{N} \sum_{m=-n}^{n} X_n^m(\eta,t) Y_n^m(\lambda,\eta)$$

Y_n^m denotes the surface spherical harmonic of degree n and order m.

$$Y_n^m(\lambda,\mu) = e^{im\lambda} \sqrt{(2n+1)\frac{(n-|m|)!}{(n+|m|)!}} \frac{1}{2^n n!} X(1-\mu^2)^{|m|/2} . \frac{d^{n+|m|}}{d\mu^{n+|m|}} (\mu^2-1)^n$$

A triangular truncation (N) is used because of its invariance through a rotation of the pole of coordinate. The right hand sides of Eqs. (2) to (4) are evaluated on a gaussian grid which has at least (3/2 N + 1) latitude circles and at least (3 N + 1) longitudes. The most interesting aspect of the model formulation is its high resolution in the stratosphere (20 levels out of 30) and the treatment of the ozone mixing ratio as a prognostic variable. The grid has been reduced to save computing time (Hortal and Simmons 1991 [16]). The vertical discretization uses a progressive hybrid coordinate taking into account the orography. The ozone mixing ratio is a prognostic variable calculated with a linearized scheme derived from a two-dimensional photochemical model (Cariolle and Déqué 1986 [4]). The time scheme is semi-implicit which is formulated as a correction to the explicit leap-frog scheme. The adiabatic equations are linearized about an isothermal dry reference of rest. The model has a comprehensive package for physical parametrizations (Mahfouf et al. 1994 [22] and Déqué et al. 1994 [7]).

3.2 *Physics*

The physics of the model allows the calculation of the different energetic exchanges between the atmosphere and the external sources (solar radiation, ocean and continents) and internal (phase changes).

- *Radiation*

  It is the most important parametrization. It is an extension and modification of the code described by Geleyn and Hollingsworth (1979 [10]) which solves the radiative transfer equation in two spectral intervals : solar (0.245μm - 4.642μm) and infrared (4.642μm - 105μm), following the delta-two-stream Eddington and adding methods. The calculation of Eddington supposes that diffusion is isotropic, only two diffusive fluxes, one upwards and the other one downwards, are considered.

  The adding method is a procedure that converts the information of each layer into a flux for the whole atmosphere. Scattering, absorption and emission by clouds, aerosols and gases H_2O,CO_2 and O_3 are taken into account. Gaseous optical depths are parametrised by Padé functions of the equivalent width. This equivalent width is obtained with a Malkmus model with continuum which takes into account the e-type and the p-type. A random overlap of adjacent cloud layers is assumed. The radiation code is called every time step allowing accurate interactions with cloud cover and the diurnal cycle.

- *Exchanges*

  - *Vertical diffusion*

    The calculations of surface and planetary boundary layer are carried out in a separate way.

    Surface

    The vertical diffusive fluxes for the variable X(wind compo-

nents, temperature and specific humidity) are calculated as:
$\overline{w'X'} = -C_X U_L (x_L - x_S)$
The subscripts S and L indicate values at the surface and at the lowest level of the model.

* w vertical velocity
* U horizontal velocity
* C_X exchange coefficient computed following Louis et al. (1982 [21])

Surface boundary layer

Following the Monin-Obukhov similarity theory

$$\frac{\partial X}{\partial z} = \frac{X_*}{k(z+z_0)} f_{bl}(\frac{z+z_0}{L_{Mo}})$$

L_{MO} Monin-Obukhov length

$$L_{MO} = \frac{c_p T U_*^2}{gkX_*}$$

z_0 roughness length. The functions (f_{bl}) are adjusted from the neutral case, using the values of the lowest model level (Geleyn 1988 [12]).

Planetary boundary layer

Following Louis (1979 [20]) and Louis et al. (1982 [21]) the exchange coefficients are function of static stability and wind shear.

$$K_x = l^2(z) ||\frac{\partial \vec{v}}{\partial z}|| f_{ex}(R_i)$$

where l is the mixing length and f_{ex} a prescribed function. The mixing length is a function of the asymptotic length l_a and of the boundary layer depth H. In the present version, l_a = 100 m and H = 1500 m

- *Horizontal diffusion*

The horizontal diffusive tendencies for the variable X: vortic-

ity, divergence, temperature, specific humidity and ozone ratio are calculated in spectral space as:

$$\frac{\partial X_n}{\partial t} = -d(n,p)X_n$$

where n is the wavenumber and d(n,p) an empirical coefficient depending on the wavenumber and the pressure. A 6th order horizontal diffusion is applied to all the prognostic variables in the troposphere. Above 100 hPa, d(n,p) increases as the inverse of pressure, so that diffusion is very strong in the top layers.

- *Convection*

  Deep convection

  It takes into account the vertical transports of moisture and heat produced by the cumulus when there is unstability. It is modelled by a mass-flux scheme with detrainment (Ph. Bougeault 1985 [2]). The deep convection takes place under two conditions: a convergence of humidity at low layers and a unstable vertical temperature profile.

  Shallow convection

  It is the non-precipitating Cu convection. Their effects are taken into account through a modified Richardson number (Geleyn 1987 [11]) which is also used in the stability computations of the gravity wave drag parametrization in order to have a consistent representation of clouds in all momentum dissipation processes. This scheme is not activated in case of very strong stability gradients.

- *Stratiform precipitation*

  This precipitation is formed when supersaturation occurs on the grid in function of temperature and mean humidity. The scheme assumes that the atmosphere is adiabatic and not allowed to become oversaturated. All the condensed water is presumed to precipitate in one time-step and precipitation is at the same temperature as the environment.

- *Gravity wave drag*

  The gravity wave drag scheme accounts for the effect of the subgrid scale orography. The gravity waves grow in amplitude as they propagate upwards, eventually becoming unstable at some height, at or near this region, the waves deposit the momentum gained at the surface.

  Three effects are taken into account in the representation of this phenomenon: dissipation, resonance and reflexion.

- *Ozone parametrization*

  The sources and sinks for ozone are parametrised by a linear dependency with temperature, total ozone and the ozone mixing ratio and the relaxation coefficients taken from a two-dimensional photochemical model (Cariolle and Déqué 1986 [4]). The full scheme includes 29 constituents, 55 chemical reactions and 20 photo-reactions. The ozone mixing ratio is treated as a prognostic variable computed by means of a transport equation.

- *Correction of negative humidity*

  The occurence of unrealistic negative values of humidity which can appear at preferential locations (near steep orography) is due to the existence of Gibbs phenomenon. Negative humidity values are corrected in each layer by evaporation from the layer below. In the bottom layer, a ficticious source of water is introduced, rather than an additional evaporation from the surface.

- *Cloudiness*

  A distinction of the radiative properties of the liquid and solid water in the clouds is taken into account.

  Stratiform cloudiness

  The stratiform cloudiness n at level l is a quadratic function of the difference between q/qsat and r_{cl} a threshold humidity profile. The cloudiness is given by the formula:

$$n_{sl} = min(n_{smax}, (\frac{\frac{q}{q_{sat}} - r_{cl}}{1 - r_{cl}})^2 i_s)$$

where n_s is the maximum cloudiness in a layer, r_{cl} is the critical humidity profile. In the cycle 11 is specified by:

$$r_{cl} = 1 - \beta_1 \frac{p}{p_s}(1 - \frac{p}{p_s})(1 + \gamma_1(\frac{p}{p_s} - \frac{1}{2}))$$

where the empirical coefficients are adjusted in order to provide a global planetary albedo of 0.30 and a balance of the global annual radiation at the top of atmosphere.

i_s is the stability index of the layer.

Convective cloudiness

The total convective cloudiness is a linear function of convective precipitation in the soil.

n_c = min (0.5,$\beta_2 F_{cp}$) if the convection is active, and $n_c = 0$ otherwise, where F_{cp}, convective precipitation, is computed at the previous time step.

β_2 = empirical coefficient (6048 mm^{-1} s).

As random overlap hypothesis is applied, the convective cloudiness is uniformly distributed among the layers. The total cloudiness is calculated by:

$$n_l = n_{sl} + (1 - n_{sl}) n_{cl}$$

- *Mesospheric drag*

  This parametrization is incorporated to avoid too strong winds and temperature in the mesosphere, but impacts on wind and temperatures down to 10 hPa. It consists of a relaxation to zero for the wind and to the standard atmosphere for the temperature.

- *Soil and vegetation*

  The vegetation soil scheme is that of Noilhan-Planton (1989 [24]). It is a parametrization of the different energetic and hydric exchanges in the surface of continents. It makes use of a minimum

number of parameters but enough in order to obtain a good characterization of physical phenomenon in the interface. It has been seen that the too warming temperatures which had been found in the surface of continents in summer are more reduced. The model calculates 5 prognostic variables: the surface temperature, the deep soil temperature, the volumetric water content of the surface, the mean volumetric water content and the water content in the interceptation reservoir.

4 1*CO_2 Climate simulation

It is necessary to prove the ability of a GCM to reproduce the present day climate before using it to simulate climate changes. The ability of this model to simulate it has been studied by Déqué and Piedelievre (1995 [8]). They verified that large-scale circulation features are correctly simulated. They focussed on the mean sea level field in the winter and summer seasons to evaluate the general circulation. The reference was the 6-year average of ECMWF analyses (1985-1991). In winter, there is a positive anomaly in the western Pacific, due to a too strong amplitude of the Pacific anticyclone but improves in the Atlantic sector.

In summer the error pattern is quite different, in the northern hemisphere the error is very large because it tends to exaggerate the Azores and Pacific anticyclones. A negative anomaly is found north Scandinavia. With respect to the local validation over Europe, where we are more interested in, the model is able to reproduce the seasonal and geographical variability of the 2m temperature over Europe. The annual bias is -0.3° C, varying between -1.6° C in summer and autumn and 1.7° C in winter. The cloud radiative forcing can explain partly the too warm 2m temperature in winter, but not the too cool summer.

The precipitation rate is not so well simulated but the geographical and seasonal variations are partly reproduced. Over southern Europe, the

summer minimum is too small. The bias is negligible when averaged over Europe, but produces local variations between -4 mm/day in winter southern Italy and 4 mm/day in summer over Norway.
The zonal component of the 10 m wind is stronger in winter, showing a mean westerly bias of 0.6 m/s. The meridional component of the 10 m wind is too southerly being the bias 1.0 m/s.
The European climate is reproduced with a generally better accuracy than other versions of the model (T42 and T106).

5 2*CO_2 Climate simulation: anomaly analyses and geographical seasonal response

5.1 *2m Temperature*

The anomalies are positive all over the area either in winter or in summer, showing the higher differences over central Europe in summer and northern Europe in winter.
In winter the anomalies increase with latitude showing the maximum values over the NE area (3° C), one reason for this could be a reduction in winter sea-ice, which could disappear completely in the Baltic sea and forms later and becomes on average thinner in the Artic Ocean, amplifying the warming of adjacent land areas, moreover northern areas are constantly snow covered so there is less evaporation, disminishing the latent heat flux in the surface heat budget. Over the rest of Europe the increase of temperature is about .5° C to 1.° C
In summer regions of largest positive anomalies are placed over central Europe (2.5°to 3.0° C) and over Iberian peninsula, southern France and Alpine region. Figures 2 show the 2m temperature anomalies distribution in winter (DJF) and summer (JJA) respectively.
Looking at the annual cycle (see Fig.3), the anomalies are mainly posi-

tive tending to follow the annual cycle, locating the maximum increases at the SW box.

5.2 *Cloud radiative forcing (CRF)*

Ramanathan (1987 [25]) developed the cloud radiative forcing concept for characterizing the relationship between clouds and the shortwave and longwave components of the radiation budget. Its main advantage is that it estimates the vertically integrated impact of clouds on radiative fluxes without having to know cloud optical properties.

CRF can be defined as the difference between the net radiation at the top of the atmosphere and the net radiation if the sky were clear. The net cloud radiative forcing is the sum of the longwave and shortwave cloud radiative forcings. Shortwave cloud radiative forcing is in general negative -clear sky albedo is less than total planetary albedo- while longwave cloud radiative forcing is in general positive. This implies heating of the earth-atmosphere system in the longwave and cooling in the shortwave.

In winter, negative anomalies dominate most of the area with the exception of the northeastern part of Finland, southwestern part of Iberian peninsula and eastern part of Balkan peninsula and Turkey.

In summer, regions of negative anomalies appear at high latitudes northwards of 58^o N latitude, as might be expected because it is in this season where the effects of persistent cloudiness and high solar insolation combine to drive the net cloud radiative forcing strongly negative (Ardanuy 1991 [1]), while regions of largest increases are located over Central Europe (21 W/m^2). These positive anomalies are not due to an increase of the cloud cover but to a different vertical distribution of the clouds.

When analysing the 2m temperature anomalies it is found that the maximum anomalies (3.5^o) are also located in Central Europe. These maxima may indicate that the positive CRF anomalies induce this warming.

Looking at the longwave and shortwave cloud radiative forcings, the area

where the net cloud radiative forcing has enhanced seems to be connected with the behavior of the anomalies in the shortwave cloud forcing, that is to say, shortwave cloud radiative forcing anomalies seem to dominate the considerably smaller longwave anomalies.

When considering the net cloud radiative forcing annual cycle (see Fig. 5), and short and longwaves cloud radiative forcings annual cycles (not shown), it is apparent the opposing nature of the shortwave and longwave forcing as is the general dominance of the shortwave term with the exception of the NE box where both anomalies are negative along the year. Figures 4 show the cloud radiative forcing anomalies distribution in winter (DJF) and summer (JJA) respectively.

5.3 *The hydrological cycle*

In winter the charts show a negative 2m relative humidity anomaly mainly over the southwest area in agreement with the areas of largest negative evaporation anomalies.

In summer negative 2m relative humidity anomaly is depicted with the maximum (-15%) placed over central Europe and a slight positive anomaly northwards, this latter anomaly is in accord with the areas of negative evaporation anomalies. Figures 6 show the evaporation anomalies distribution in winter (DJF) and summer (JJA) respectively and Figure 7 the corresponding annual cycle.

Analysing the total precipitation anomalies, it is found in winter, negative values with the minimum value, -2.0 mm/day, placed western Scotland and -1.0 mm/day central Europe, mainly due to the lack of the stratiform precipitation. The largest positive anomalies, 2.0 mm/day, are placed over Scandinavian peninsula and the NE area.

In summer, all Europe shows negative values except some areas over Scandinavian peninsula and the NE area. The maximum negative anomalies, -2.0 mm/day, are placed over the Alps and the Balkan regions, in

this case there is a contribution of either stratiform or convective precipitation. Figures 8 show the total precipitation anomalies distribution in winter (DJF) and summer (JJA) respectively. Looking at the annual cycle (see Fig. 9), there is a deficit of precipitation in all the boxes from June to September, the maximum negative anomaly, -1.2 mm/day, is placed over the NW box in August. In the SW box the negative anomaly is prolonged from April to January, showing in March the maximum positive anomaly 1.4 mm/day of Europe.

5.4 *Mean sea level pressure*

In winter the anomaly is positive all over the area increasing with latitude, being located the maximum value (5 hPa) northern Atlantic, over Iceland. while in summer the anomaly is mainly zero.

5.5 *10m Wind*

In winter the anomaly is northwesterly northern Europe, mainly due to the positive mean sea level pressure anomaly, easterly over the British Isles and Netherlands and mainly zero over the rest of Europe, showing the maximum value western British Isles. In summer the anomaly is mainly zero all over Europe, with the exception of a southerly anomaly northern Iberian peninsula. Figures 10 show the 10m wind anomalies distribution in winter (DJF) and summer (JJA) respectively.

5.6 *Height fields*

5.6.1 *Geopotential*

The anomaly is positive increasing with latitude in winter either at 500 and 850 hPa, locating the maximum value (80 hPa) at 500 hPa northern Great Britain. In summer the maximum increase is at 500 hPa placed northern Iberian peninsula (62 hPa) and southern France. Figures 11 show the 500 hPa geopotential height anomalies distribution in winter (DJF) and summer (JJA) respectively.

5.6.2 *Wind*

In the winter stratosphere (1,10, 50 and 200 hPa) the anomaly is westerly northern Europe and easterly central and southern Europe. These differences increase with altitude and latitude showing the maximum values northern Europe (6 m/s) at 200 hPa, the minimum value, near zero, is placed over central Europe at 50 hPa. In summer the anomaly is westerly all Europe increasing with latitude and altitude showing the maximum value (2 m/s) northwards. Analysing the wind components along the annual cycle the most important differences are mainly due to the zonal component, showing the maximum differences in winter.

In the winter troposphere (500 and 850 hPa) the anomaly is northwesterly northern Europe turning to easterly central Europe and British Isles, southerly southeastern Europe and near zero over the Iberian peninsula, these differences increase with altitude and the maximum value (4 m/s) is placed over the British Isles.

In summer the anomaly is southwesterly over the British Isles, easterly northwestern Europe turning to northerly northwestern and central eastern Europe, northwesterly southern Europe and near zero over France and the Netherlands. These differences increase with altitude being the maximum values, 4 m/s, placed northern and western Europe and west-

ern British Isles. Analysing the wind components along the annual cycle the maximum differences are due to the meridional component for the northern boxes and to the zonal component for the southern boxes at 200 and 500 hPa. Figures 12 show the 500 hPa wind anomalies distribution in winter (DJF) and summer (JJA) respectively.

5.6.3 *Temperature*

There is a clear warming in the troposphere and a cooling in the stratosphere. The warming in the troposphere is due not only to the CO_2 increase but to an enhancement of the water vapor greenhouse as well, driven by the SST positive anomalies. The anomalies at the levels: 500, 700 and 850 hPa are always positive either in winter or in summer.
When analysing the annual cycle the maximum values (3.6° C) are located at 500 hPa in March in the SE box, the minimum value 0.0° C occurs at 850 hPa in August in the SE box. This increase with altitude may be due to the warming at low levels that enhances the surface evaporation leading to a more intense convective activity with the corresponding increase of latent heat and humidity at high pressure levels. Figures 13 show the 500 hPa temperature anomalies distribution in winter (DJF) and summer (JJA) respectively.
The cooling in the stratophere is due to the increase of CO_2 which enhances the cooling to space effect in the LW emission. This cooling increases with altitude, from 10 to 1 hPa, showing the maximum negative values northern Europe late winter, $-13.0°$ C in the NE box. This strong cooling may have not a radiative but a dynamic origin, it may come from a sudden warming in the 1^*CO_2 simulation and an inhibition of it in the 2^*CO_2 experiment during winter.
It is well known that in the northern hemisphere, the winter circulation at high latitudes is disturbed from radiative equilibrium by the planetary waves activity that propagates upwards out of the troposphere (Trenberth, 1992 [32]). Sporadically, the amplitudes of these waves amplify

dramatically leading to a breakdown of the polar vortex and to a strong and abrupt temperature increase in the stratosphere, the so-called sudden warmings.
At 50 hPa it is found a positive anomaly (2.5° C) in February at northern boxes, this may be due to a sudden warming that appears either in $1*CO_2$ or $2*CO_2$, being enhanced in the $2*CO_2$ simulation.

These sudden warmings have important consecuences in stratosphere dynamics as it is seen when analysing the ozone. Figures 14 show the 50 hPa temperature anomalies distribution in winter (DJF) and summer (JJA) respectively and Figure 15 the corresponding annual cycle.

5.6.4 *Ozone*

Tropospheric changes due to increased CO_2 may affect planetary waves propagation and can alter the stratosphere dynamics. Moreover, these perturbations can lead more or less directly to changes in atmospheric composition and chemistry (Rind et al. 1990 [26]).
Due to the fact that the ARPEGE model has good resolution in the stratosphere and mesosphere (20 levels) it will allow us to study the impact of the CO_2 increase on the homogeneous chemistry and the dynamics of the stratosphere (Timbal et al. 1995 [31]).
As previously mentioned, the CO_2 increase enhances the cooling to space effect in the longwave emission and leads to a cooler stratosphere. A cooler stratosphere would tend to reduce the efficiency of many catalytic O_3 removal cycles, resulting in an increase of ozone concentration.
When analysing the seasonal cycle of ozone mixing ratio anomalies (50, 10, 1 hPa), it becomes clear that all the subdomains show positive anomalies, with the highest values late winter and early spring, 0.52 ppmv at 1 hPa, 1.15 ppmv at 10 hPa, 0.65 ppmv at 50 hPa for the northern boxes, the minimum anomaly, 0.05 ppmv, is located at 10 hPa in April. Figures 16 show the 50 hPa ozone anomalies distribution in winter (DJF)

and summer (JJA) respectively and Figure 17 the corresponding annual cycle.

This increase in O_3 in the upper stratosphere produces a shadowing effect on the local UV flux, this implies a less efficient oxygen photodissociation in the upper troposphere, which means a lesser increase in O_3. This is in agreement with our results since at 200 hPa we have obtained 0.1 ppmv as the maximum value late winter.

5.7 *Total ozone*

On the basis of photochemical considerations, one would expect the greatest ozone content at low latitudes where the UV flux is largest and where most stratospheric ozone is produced. Actually, column abundances are largest at middle and high latitudes. This fundamental discrepancy can be explained only by incorporating dynamical effects.

Analysing the geographical distribution of anomalies of the ozone content integrated over the vertical column for winter period, the anomalies are strongly positive, increasing northwards, displaying the maximum values at high latitudes, eastward of Gulf of Finland (30 Dobson units), due to poleward and downward ozone transport. In summer the anomalies are also positive but slightly smaller, increasing northwards. This increase in the O_3 anomaly supports the primary conclusions of two dimensional photochemical stratospheric models which demonstrated that the cooling of the lower stratosphere reduces the efficiency of ozone destruction, predicting however a smaller increase of the column abundance of ozone by a doubling of CO_2, as indicated by Brasseur and Hitchman (1988 [3]). This may be due to the stratospheric dynamics modification during winter that did not occur in simpler models.

6 Summary and conclusions

In this work we have discussed a climate change scenario over Europe induced by the doubling of CO_2 concentration. To do this we have used the stretched version of the ARPEGE climate model (T63s) and a monthly SST anomaly from a scenario simulation by the Max Planck Institute. We focus our study on the anomalies obtained from five annual cycles of the control and the doubled CO_2 simulations.
The results can be summarized as follows:

- Warming in the troposphere and a cooling in the stratosphere. The warming in the troposphere is due not only to the CO_2 increase but to an enhancement of the water vapor greenhouse as well, driven by the SST positive anomalies.
  The cooling in the stratosphere is caused by the CO_2 increase which enhances the cooling to space in the longwave emission. The anomalies increase with height, maximum negative values are located northern Europe late winter.

- Increase in the ozone mixing ratio at 1, 10 and 50 hPa. All subdomains show positive anomalies with the highest values late winter and early spring for the northern subdomains.

- Increase in the total ozone. Anomalies tend to increase northwards, being especially stronger in winter.

- For the cloud radiative forcing, anomalies are mainly negative in winter all over the considered area with the exception of northeastern Finland, southwestern Iberian peninsula and eastern Balkan peninsula and Turkey. In summer negative anomalies 58 ° northwards, and large positive anomalies central Europe.

- For the 2m temperature, in winter there is shown a very slight warming. Anomalies increase with latitude being the maximum

values located over the NE subdomain.

These results may be compared with those obtained by Giorgi et al. (1992 [14]), with a Limited Area Model (MM4) nested in a General Circulation Model (Community climate model (CCM) of the NCAR). For January they obtained a warming in the range of 3 °C southern Europe to 5.0 °C northern British Isles and northwestern Scandinavian peninsula, whereas for winter (DJF) we obtained warmings from 0.5 ° southern and central Europe, to 1 °C northern British Isles and from 1.5 to 3.0 °C northern Europe. This less warming may be explained, partialy by the northerly wind anomaly we obtained over Europe.

For July they obtained a warming in the range of 2 °C western Europe to 5 ° C eastern Europe, with the maximum warming of 6 °C over the Scandinavian peninsula, whereas for summer (JJA) we obtained warmings from 2.5 °C to 3.0 °C central Europe, France and Iberian peninsula. The maximum warming 3.5 °C is placed over the Alpine region.

So they obtained a warming over Europe in all seasons which is in the range of 1.5°C to 7.0 °C, while we obtained an average warming of 1.55 °C over Europe.

Considering the work of Gregory and Mitchell (1995 [15]), a $2CO_2$ simulation of surface temperature and precipitation over Europe using the UKMO climate model, it is notorious the difference in the 2m temperature. They obtained a warming from 3 K in Turkey to 10 K in the region of Scandinavia in winter and from 4 K northern Europe to 8 K southern Europe in summer.

- For the total precipitation the main positive anomalies take place eastern Scandinavian peninsula either in winter or in summer whereas the main negative anomalies are located over the Alpine region in summer.

  Comparing these results with the MM4/CCM (Giorgi et al. 1992 [14]), they predict for January a decrease of precipitation over south-

ern Scandinavian peninsula (-1 mm/day), extended areas of the Balkan region, southern England, central France (-0.5 mm/day), and northwestern Iberian peninsula, whereas for winter (DJF) we obtained negative values over central Europe, the Balkan region, western Italy, some areas of France and Denmark, and the British Isles. So we obtained quite similar negative areas, being the positive areas much more enhanced in the MM4/CCM simulation.
Referring to July the differences are more notorious, MM4/CCM showed positive values all over Europe with the exception of some little areas of the Balkan region, Latvia and Lithuania whereas for summer (JJA) we obtained negative values all over the considered area with the exception of a little area northwestern Spain and western Scandinavian peninsula (1.4 mm/day). The most noticieable difference is the maximum they obtained over the Alpine region (2.7 mm/day) in contrast with the minimum we found in this area (-2.0 mm/day). The only agreement occurs at Great Britain where both have obtained negative values. Averaging over all land grid points they obtained a percentage precipitation increase of 11.5 % while we obtained a decrease of -11% , this difference is mainly due to the summer months.

In Table 1 it is shown the main annual-mean anomalies for the four european boxes (NW, NE, SW and SE) and the full domain (EUR).

Thus, our results yield a climate change scenario, somewhat different from other authors. These discrepancies would be probably due mainly to the deficiencies and differences in the control simulations of the present climate. In this way and with respect to the surface temperature Marinucci and Giorgi (1992 [23]) obtained a cold bias in winter and a warm bias in summer whereas Déqué and Piedelievre (1995 [8]) obtained opposite biases and the same as for precipitation.
Another important source of discrepancies may arise from the SST and

sea-ice fields considered in each experiment due to the undoubtful influence they exert on climate.

Therefore more effort would be needed to improve the ability of GCMs to simulate regional climates and so increase the confidence in the projection of regional responses to climate change.

7 Acknowledgements

The authors are indebted to Météo France for the use of the climate GCM ARPEGE model and especially to Michel Déqué for his continous support and useful comments. Thanks also to Alain Braun for his technical help at Météo France.

8 References

References

[1] Ardanuy P.E, Stone L.L, Gruber A.,1991: Shortwave, Longwave and Net Cloud Radiative Forcing as determined from Nimbus 7 Observations. *J. Geophys. Res.*, **96**, 18537-18549.

[2] Bougeault Ph., 1985: A simple parameterization of the large-scale effects of deep cumulus convection. *Mon. Wea. Rev.* ,**113**, 2108-2121.

[3] Brasseur G, Hitchman,1988: Stratospheric response to trace gas perturbati on changes in ozone and temperature distributions. *Science* ,**240**, 634-637.

[4] Cariolle D, Déqué M,1986: Southern Hemisphere medium-scale waves and total ozone disturbances in a spectral genaral circulation model. *J. Geophys. Res.*, **91**, 10825-10846.

[5] Courtier P, Geleyn JF. 1988: A global numerical weather prediction model with variable resolution: application to the shallow water equations. *Q.J.R. Meteorol. Soc.*, **117**, 1057-1080.

[6] Cubasch U., Hasselmann K., Höck H., Maier-Reimer E., Mikolajewicz U., Santer B.D., and Sausen R. 1992: Time-Dependent Greenhouse Warming Computations with coupled Ocean-Atmosphere Model. *Climate Dyn.* **8**, 55-69.

[7] Déqué M, Dreveton C, Braun A, Cariolle D., 1994: The ARPEGE/IFS atmosphere model: a contribution to the French community climate modelling. *Climate Dyn.*.**10**, 249-266.

[8] Déqué M, Piedelievre JPh. 1995: High resolution climate simulation over Europe. *Climate Dyn.*,**11**, 321-339.

[9] DOE. 1990: *Energy and Climate Change.* MacCracken, Luther, Eds, U'S Department of Energy.

[10] Geleyn JF., Hollingsworth A., 1979: An economical analytic method for the computation of the interaction between scattering and line absorption of radiation. *Beitr. Phys. Atmos.*,**52**, 1-16.

[11] Geleyn JF.,1987: Use of a modified Richardson number for parameterizing the effect of shallow convection. *J. Meteorol. Soc. Japan Spec NWP symposium volume* , 141-149.

[12] Geleyn JF.,1988: Interpolation of wind, temperature and humidity values from model levels to the height of measurement. *Tellus*, **40A**, 347-351.

[13] Giorgi F.,1990: Simulation of regional climate using a limited area model nested in a general circulation model. *J. Climate* ,**3**, 941-963.

[14] Giorgi F, Marinucci M.R., Visconti G.,1992: A $2CO_2$ Climate change Scenario over Europe generated using a limited area model nested in a general circulation model. II Climate change scenario. *J.Geophys. Res.,* **97**, 10011-10028.

[15] Gregory J.M., Mitchell J.F.B., 1995: Simulation of daily variability of surface temperature and precipitation over Europe in the current and $2CO_2$ climates using the UKMO climate model. *Q.J.R. Meteorol. Soc.*,**121**, 1451-1476.

[16] Hortal M., Simmons AJ.,1991: Use of reduced Gaussian Grids in Spectral Models. *Mon. Wea. Rev.*,**119**, 1057-1074.

[17] Intergovernmental Panel on Climate Change, 1990:*Climate Change. The IPCC Scientific Assessment.* J.T. Houghton, G.J. Jenkins, and J.J. Ephraums, Eds., Cambridge University Press, 365pp.

[18] Intergovernmental Panel on Climate Change, 1992:a*Climate Change. Supplementary Report to the IPCC Scientific Assessment.* J.T. Houghton, G.J. Jenkins, and J.J. Ephraums, Eds., Cambridge University Press.

[19] Kiehl JT., Ramanathan V.,1990: Comparison of cloud forcing derived from the Earth Radiation Budget Experiment with that simulated by the NCAR Community Climate Model. *J. Geophys. Res.*, **95**, 11679-11698.

[20] Louis JF., 1979: A parametric model of vertical eddy fluxes in the atmosphere. *Bound Layer Meteorology***17**, 187-202.

[21] Louis JF., Tiedke M., Geleyn JF., 1982: A short history of the PBL paramete rization at ECMWF. Proceedings of the ECMWF workshop on planetary boundary layer parameterization. Reading, 25-27 Nov. 1981, 59-80

[22] Mahfouf JF., Cariolle D., Royer JF., Geleyn JF., Timbal B., 1994: Response of the Meteo-France climate model to changes in CO_2 and sea surface temperature. *Climate Dyn.,* **9**, 345-362.

[23] Marinucci M.R., Giorgi F., 1992: A $2CO_2$ Climate change Scenario over Europe generated using a limited area model nested in a general circulation model. I: Present day simulations. *J.Geophys. Res.,* **97**, 9989-10009.

[24] Noihlan J., Planton S., 1989: A simple parameterization of land surface processes for meteorological models. *Mon. Wea. Rev.,* **117**, 536-549.

[25] Ramanathan V. 1987: The role of Earth radiation budget studies in climate and general circulation. *J. Geophys. Res.*, **92**, 4075-4095.

[26] Rind D., Suozzo R., Balachandran NK., Prather MJ., 1990: Climate Change and the Middle Atmosphere. Part I: The Doubled CO_2 Climate. *J. Atmos. Sci.*, **47**, 475-494.

[27] Simmons AJ., Burridge D..1981: An energy and angular momentum conserving vertical finite difference scheme and hybrid vertical coordinates. *Mon. Wea. Rev.*, **109**, 758-766.

[28] Schmidt F. 1977: Variable fine mesh in spectral global model. *Beitr. Phys. Atmos.*, **50**, 211-217.

[29] Staniforth AN., Mitchell HL., 1978: A variable-resolution finite element technique for regional forecasting with the primitive equations. *Mon. Wea. Rev.*, **106**, 439-447.

[30] Timbal B, Mahfouf JF (1992) Analyse d'une expérience de sensibilité au doublement du CO_2 avec le modéle Emeraude. Note de centre N 15 CNRM/METEO-FRANCE.

[31] Timbal B., Mahfouf JF., Royer JF., Cariolle D., 1995: Sensitivity to prescribed changes in sea surface temperature and sea ice in doubled carbon dioxide experiments *Climate Dyn.*, **12**, 1-20.

[32] Trenberth KE., 1993: *Climate System Modeling.* Cambridge University Press, 788 pp.

9 List of Figures

List of Figures

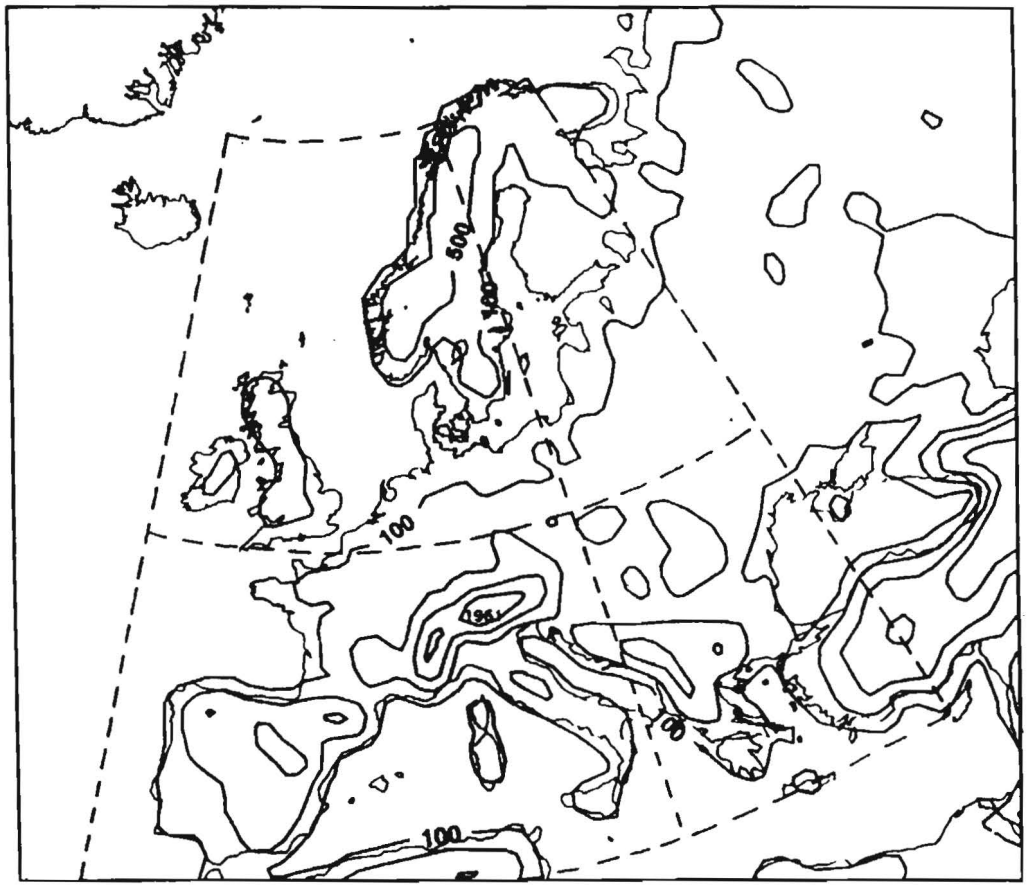

Figure 1: **Orography** of the T63s and the boundaries of the four sub-domains. The plotted contours are 100, 500 1000 and 1500 m.

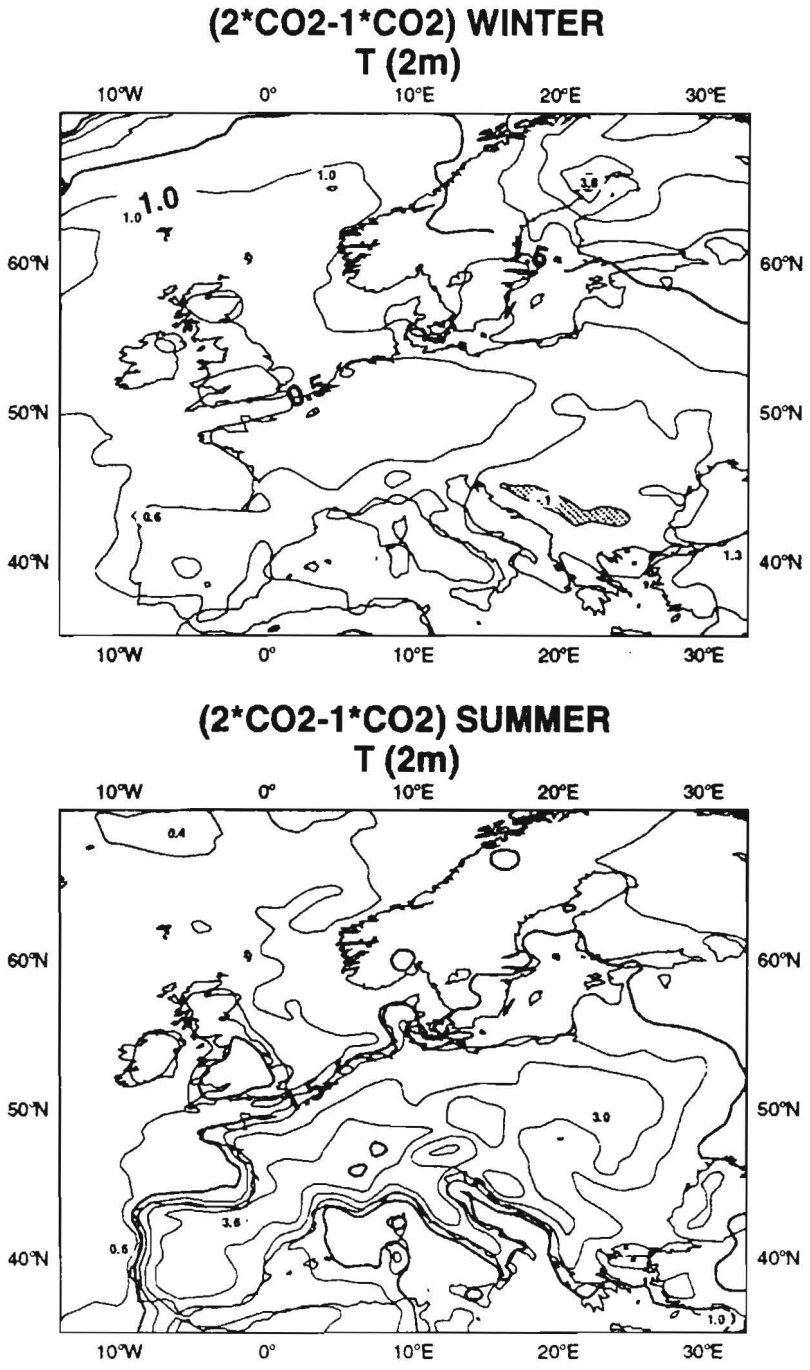

Figure 2: Anomalies of the **2m Temperature** for winter and summer. The contour interval is 0.5°C, the negative values are shaded.

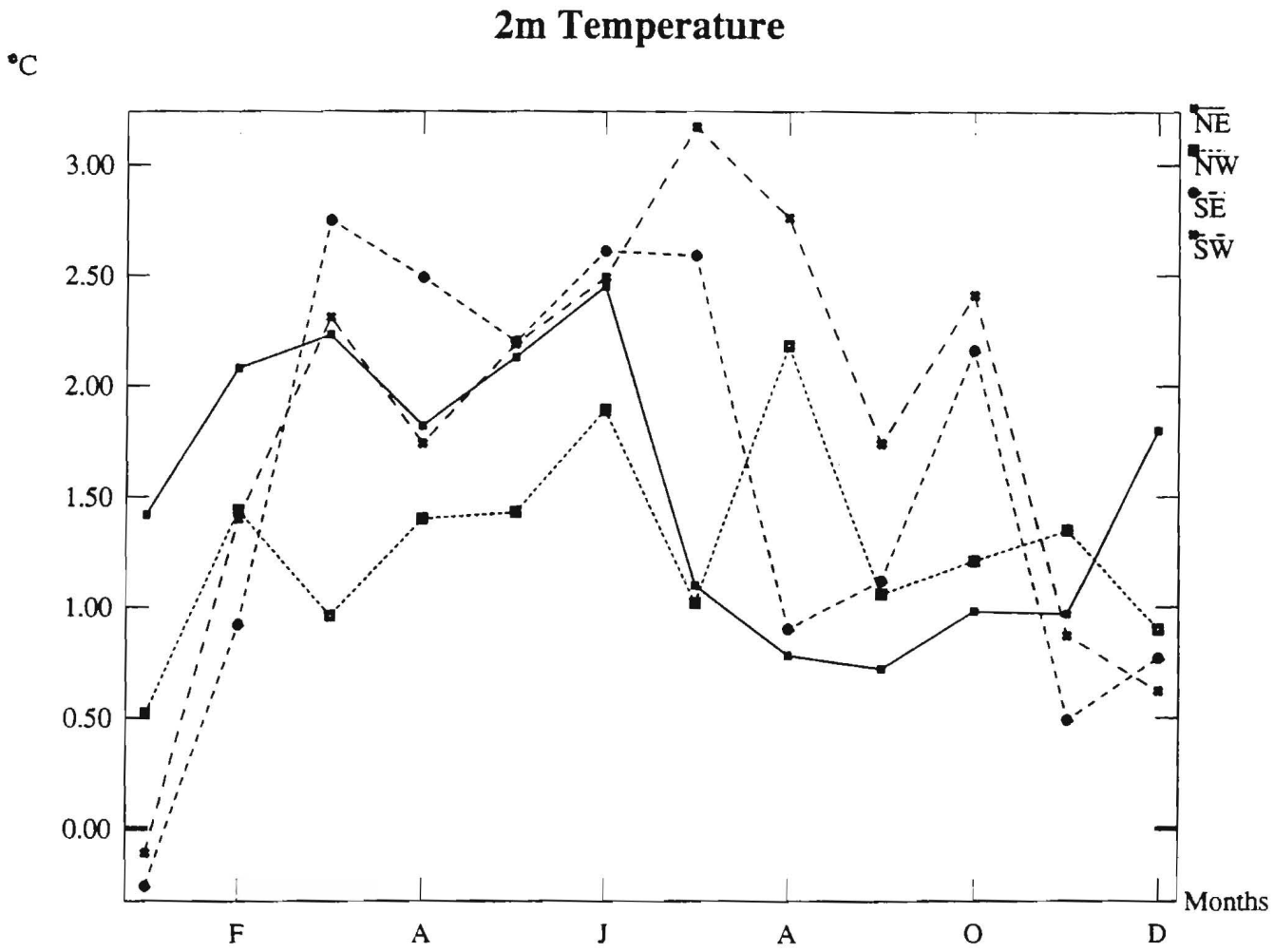

Figure 3: Anomaly monthly mean **2m Temperature** (°C) for the four European subdomains (NW, NE, SW and SE)

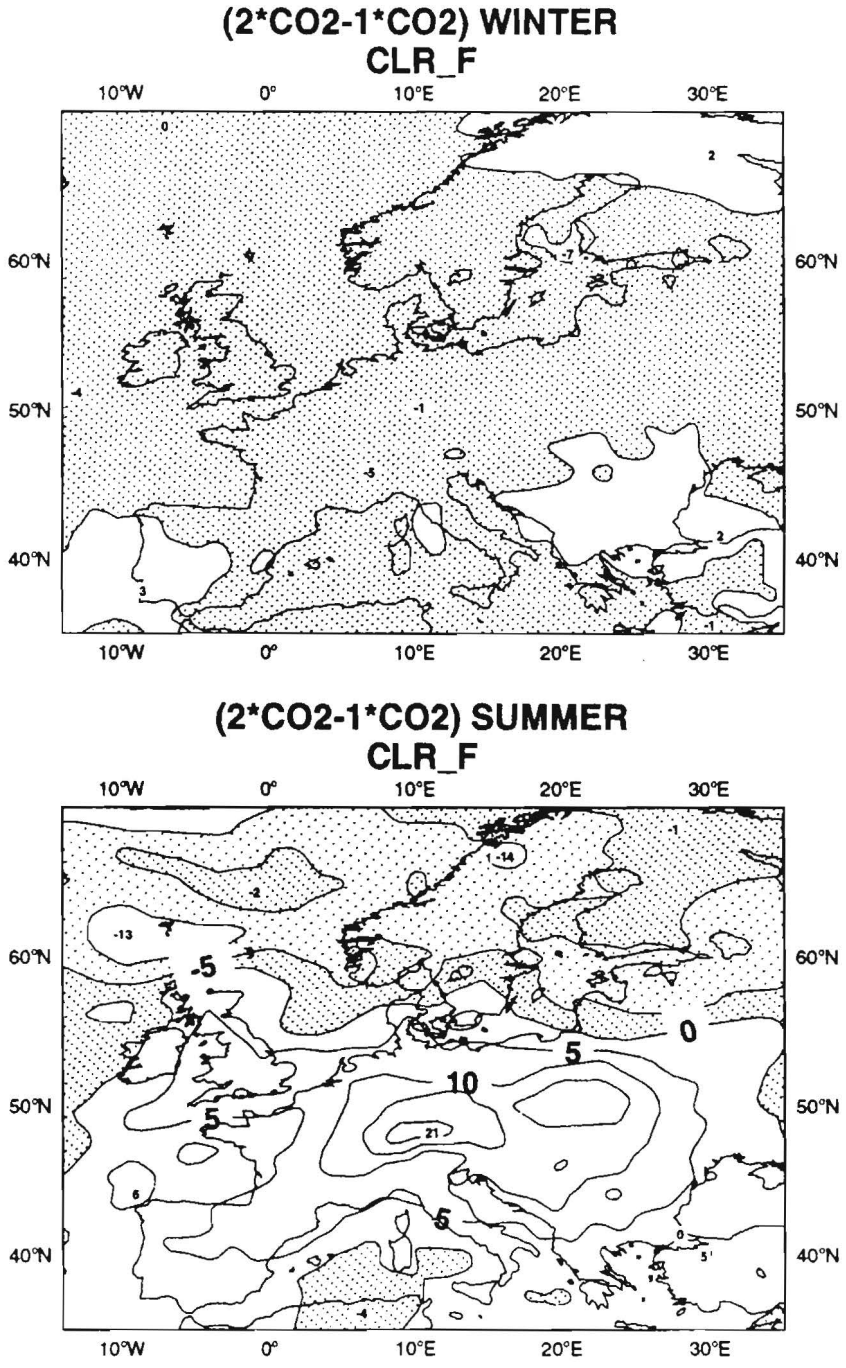

Figure 4: Anomalies of the **Cloud Radiative Forcing** for winter and summer. The contour interval is 5.0 W/m^2, negative values are shaded.

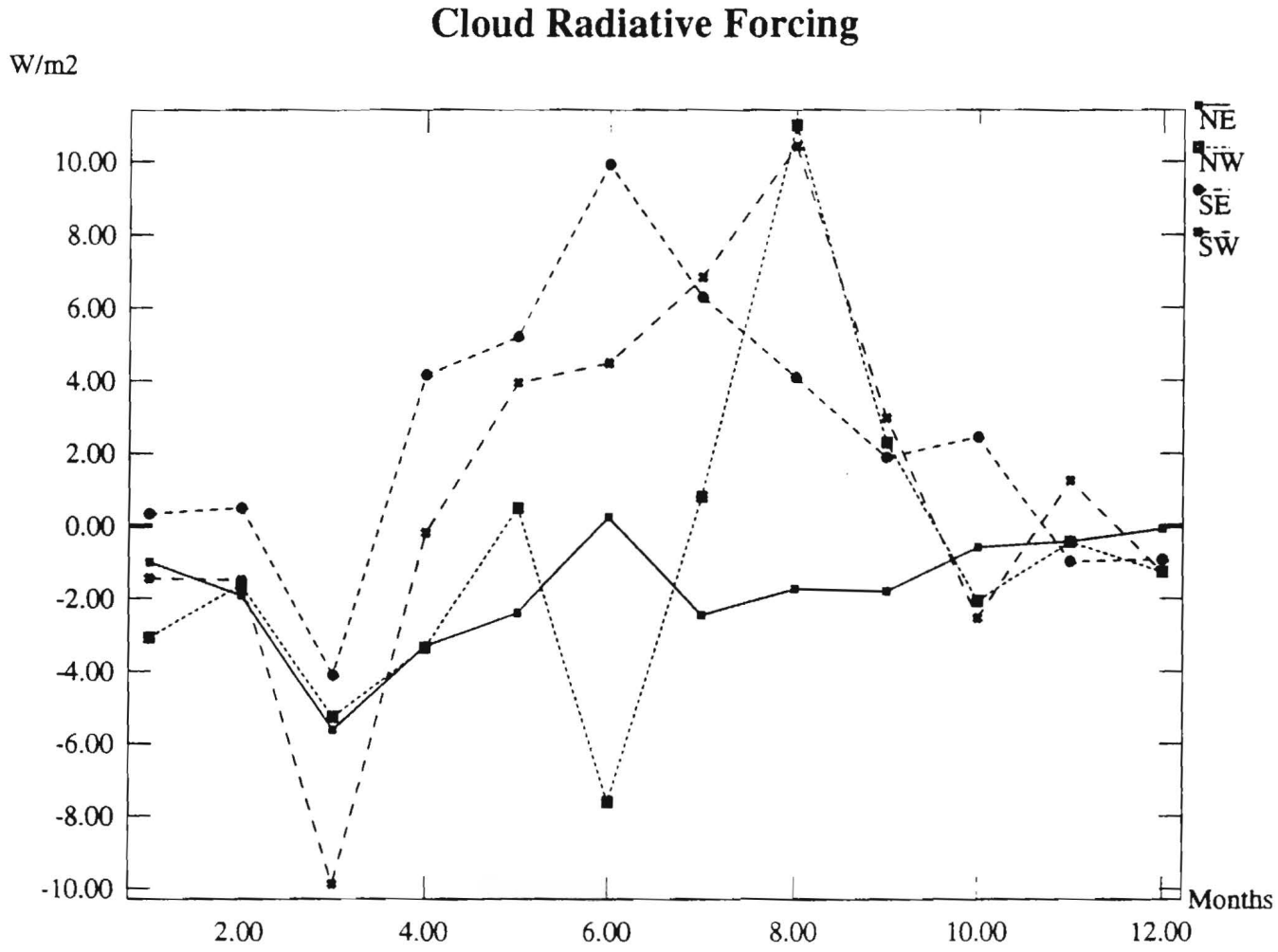

Figure 5: Anomaly monthly mean **Cloud Radiative Forcing** (W/m^2) for the four European subdomains (NW, NE, SW and SE)

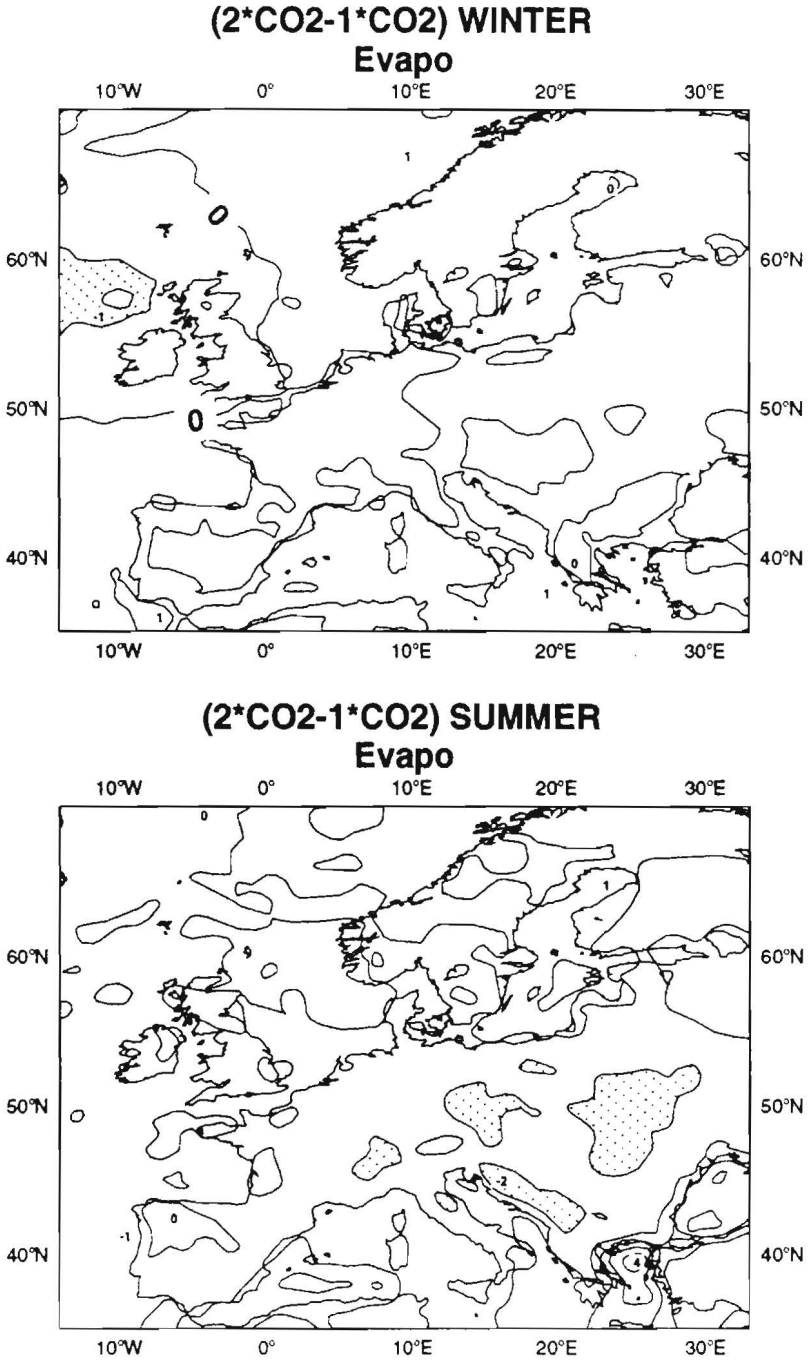

Figure 6: Anomalies of the **Evaporation** for winter and summer. The contour interval is 1.0 mm/day, negative values are shaded.

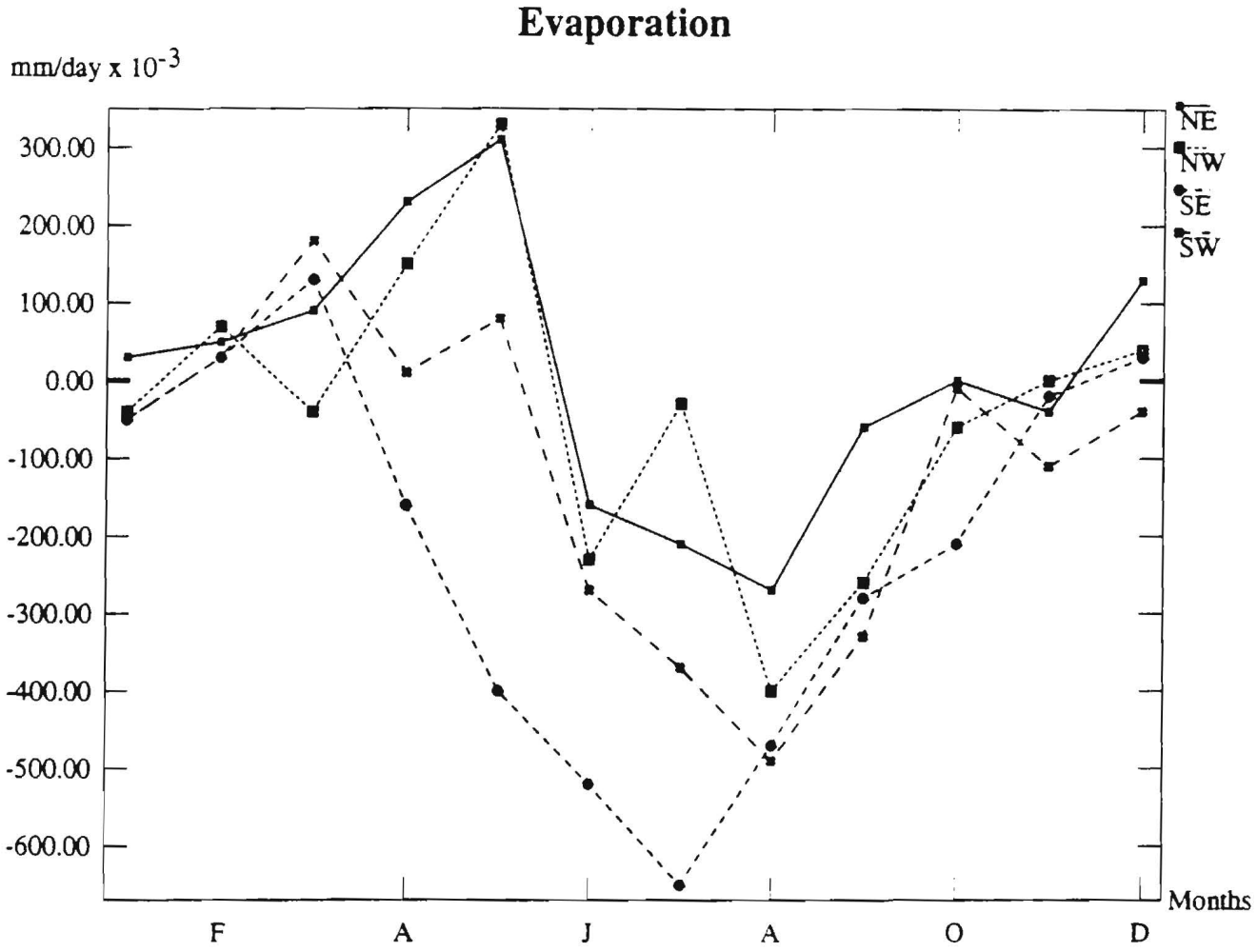

Figure 7: Anomaly monthly mean **Evaporation** (mm/day) for the four European subdomains (NW, NE, SW and SE)

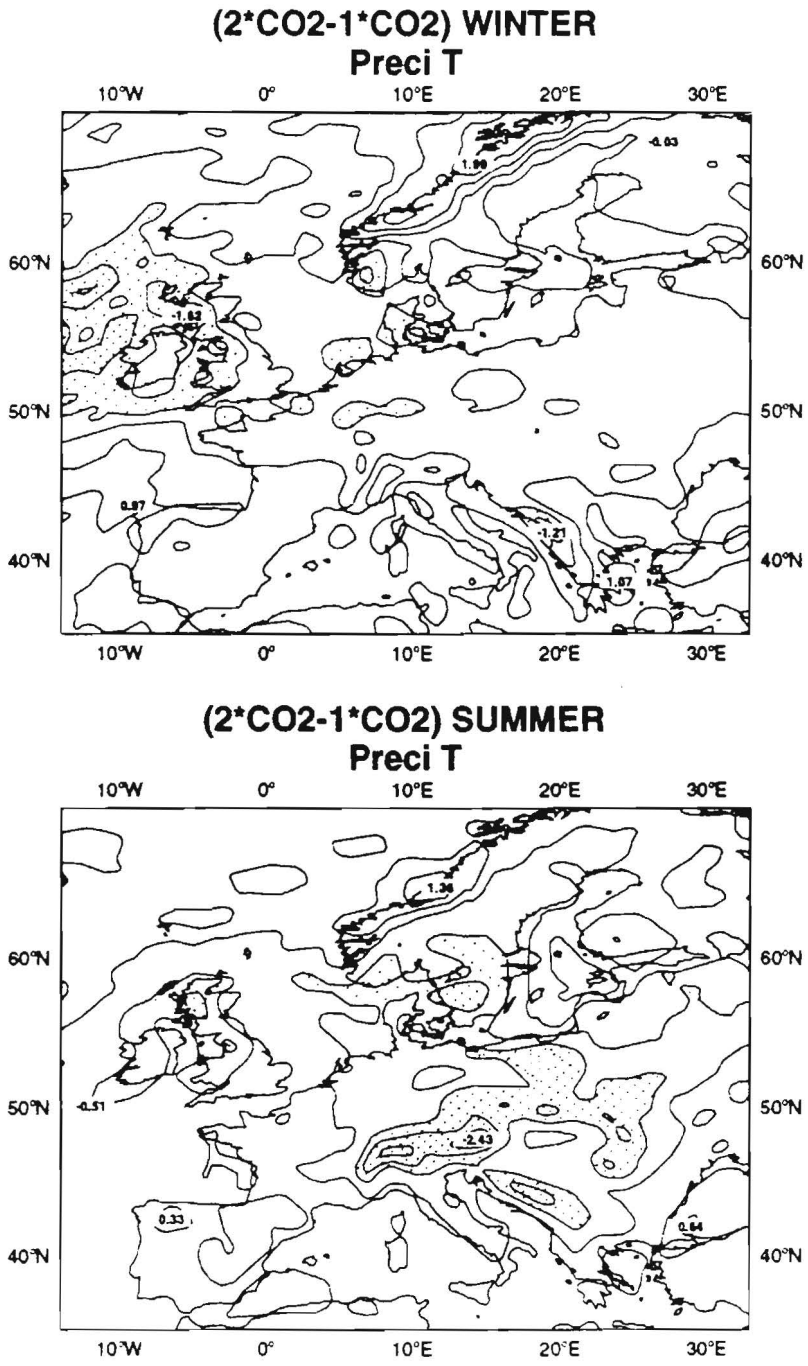

Figure 8: Anomalies of the **Total Precipitation** for winter and summer. The contour interval is 0.5 mm/day, negative values are shaded.

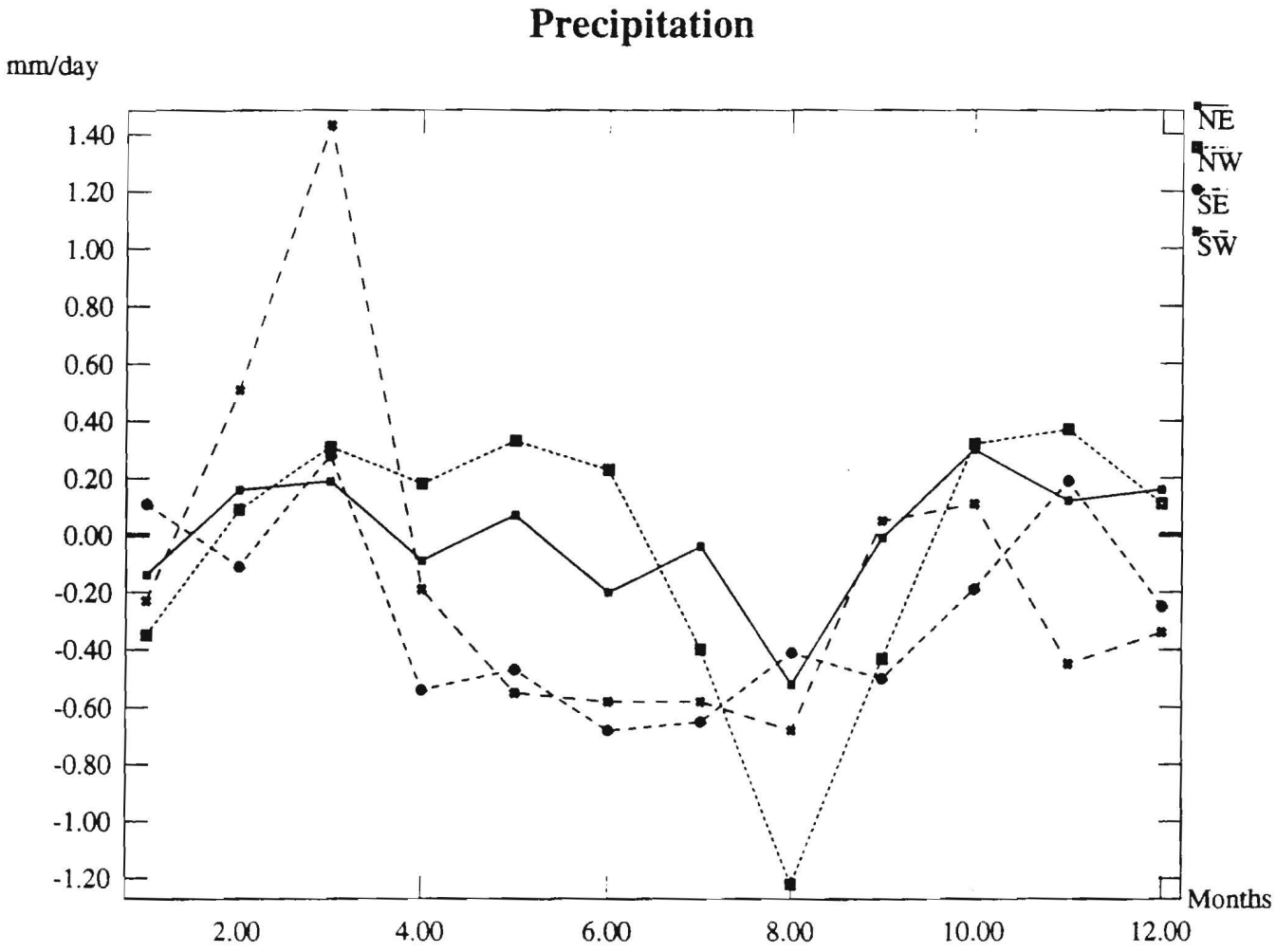

Figure 9: Anomaly monthly mean **Total Precipitation** (mm/day) for the four European subdomains (NW, NE, SW and SE)

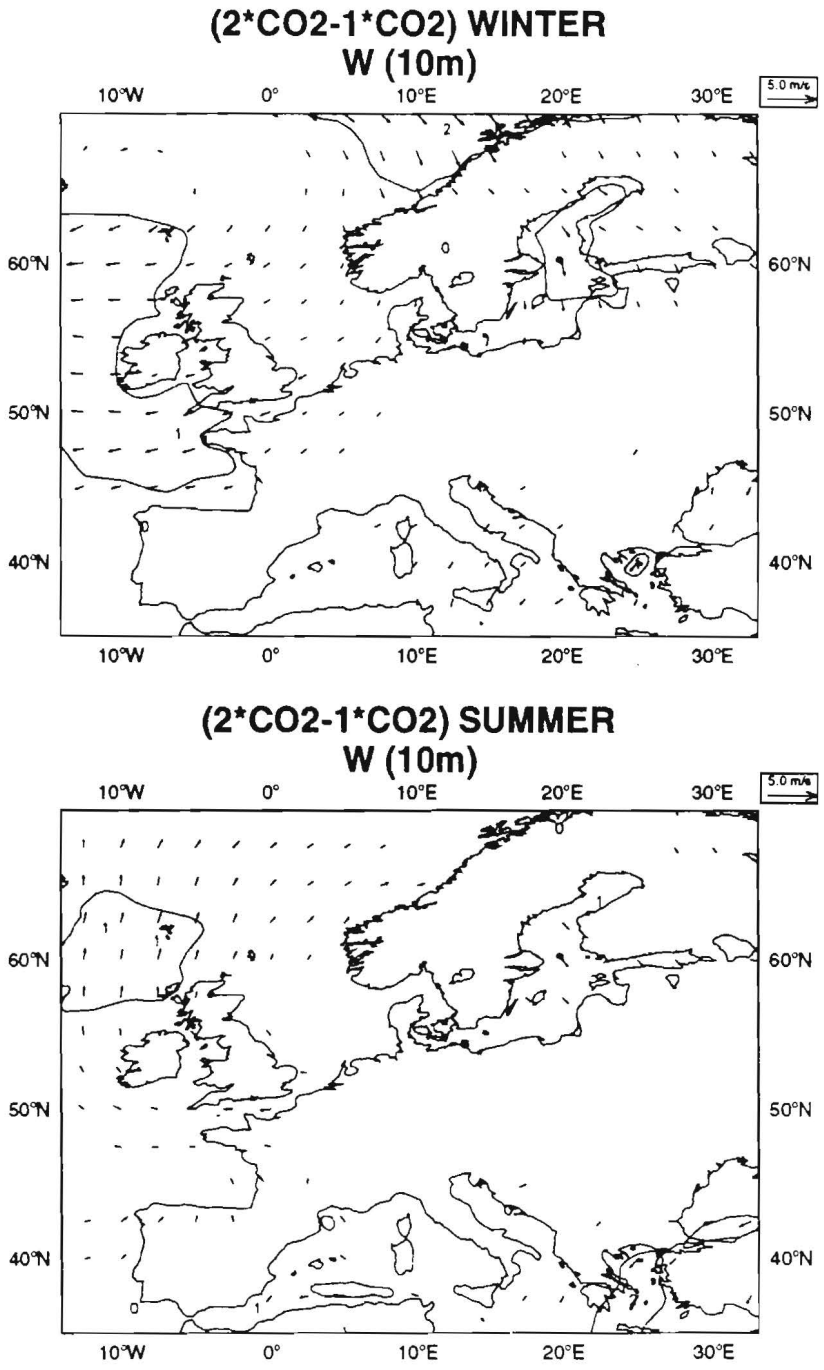

Figure 10: Anomalies of the **10m Wind** for winter and summer. The contour interval is 1.0 m/s, negative values are shaded.

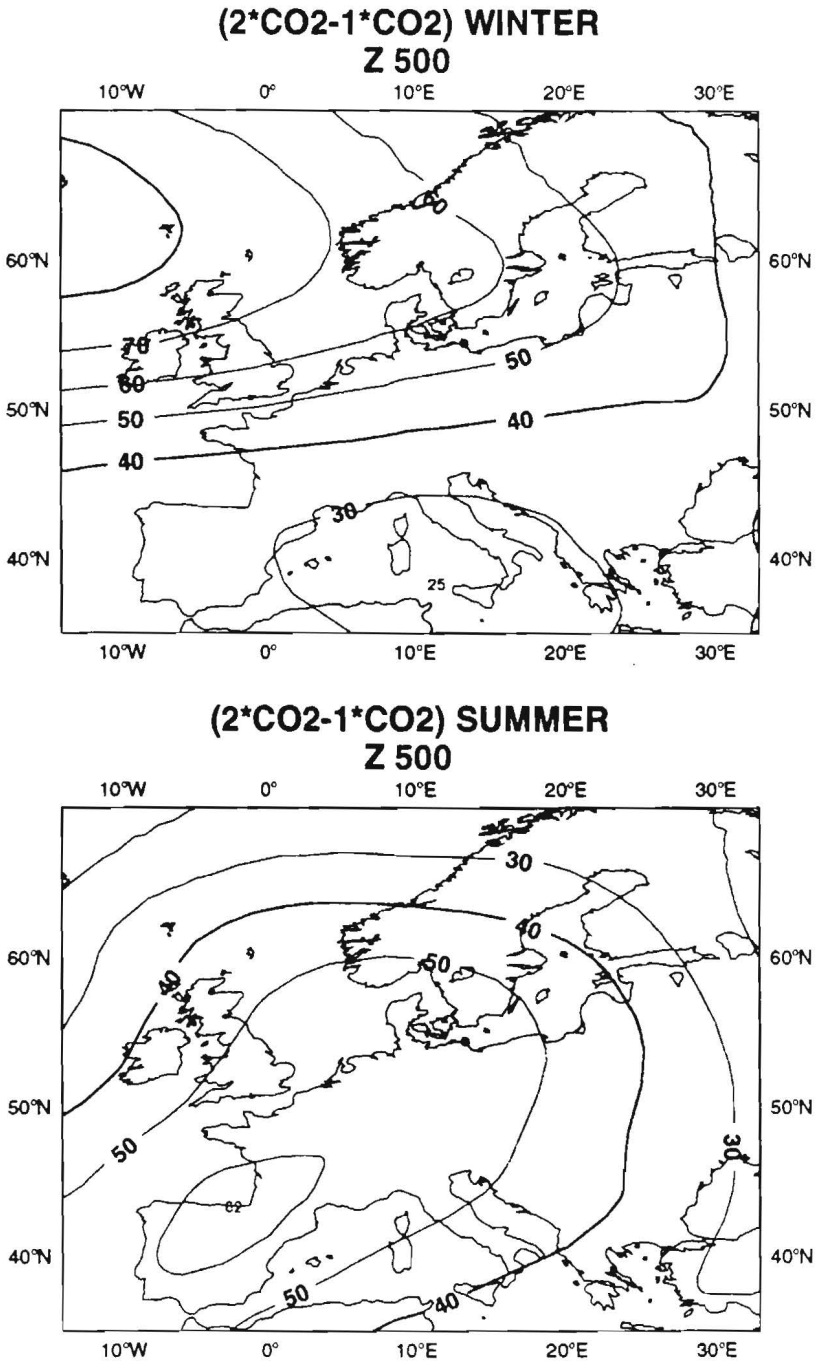

Figure 11: Anomalies of the **500 hPa Geopotential height** for winter and summer. The contour interval is 10 m, negative values are shaded.

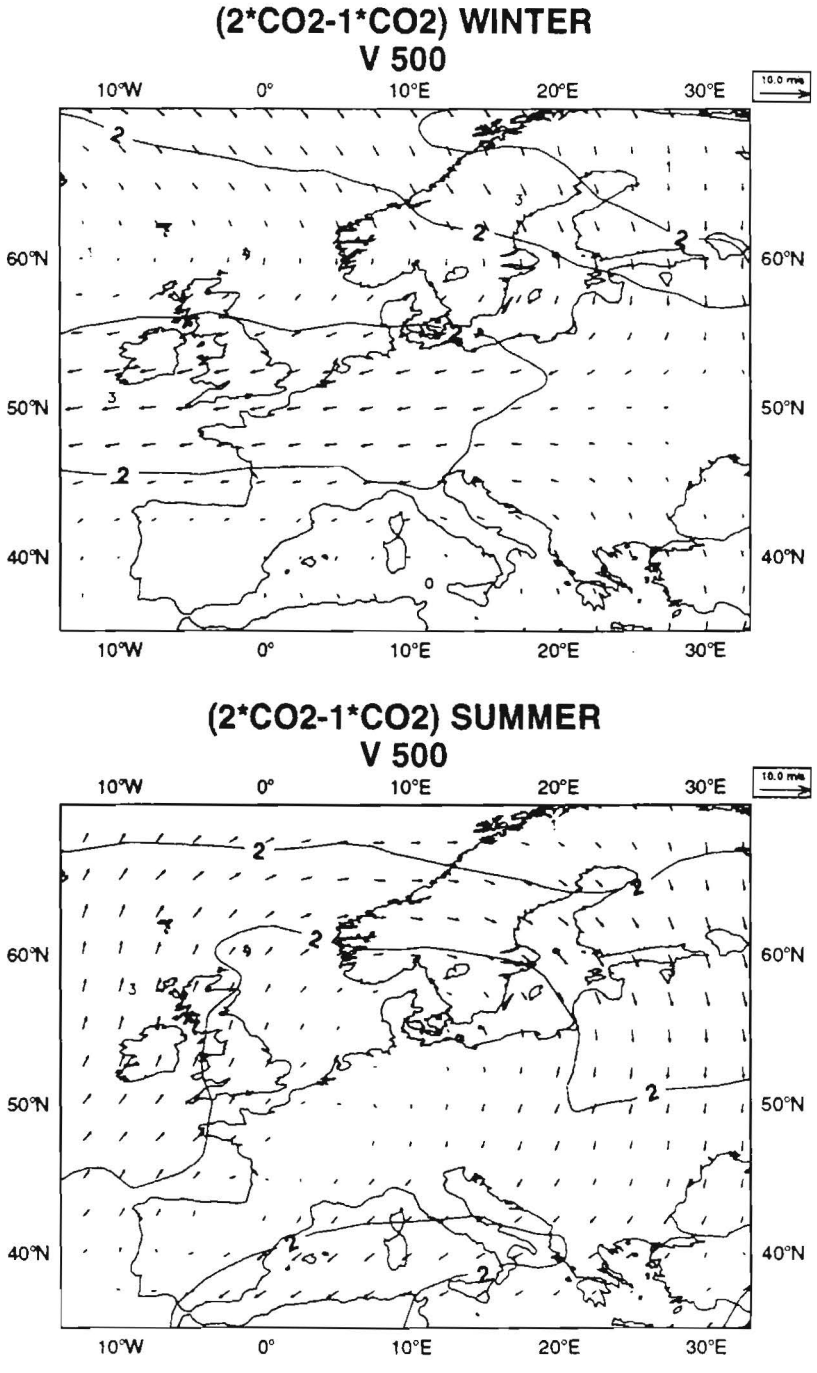

Figure 12: Anomalies of the **500 hPa Wind** for winter and summer. The contour interval is 2 m/s, negative values are shaded.

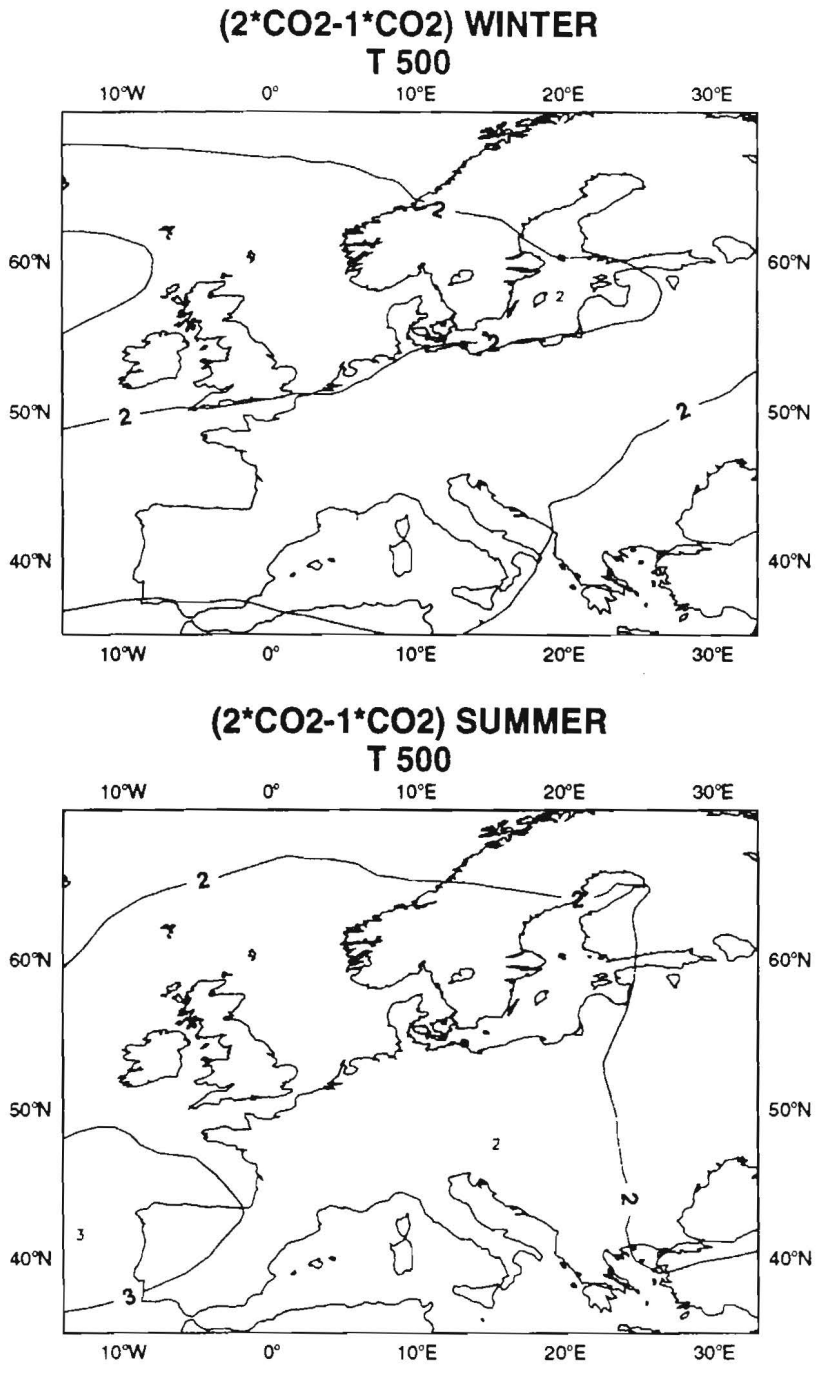

Figure 13: Anomalies of the **500 hPa Temperature** for winter and summer. The contour interval is 1.0°C.

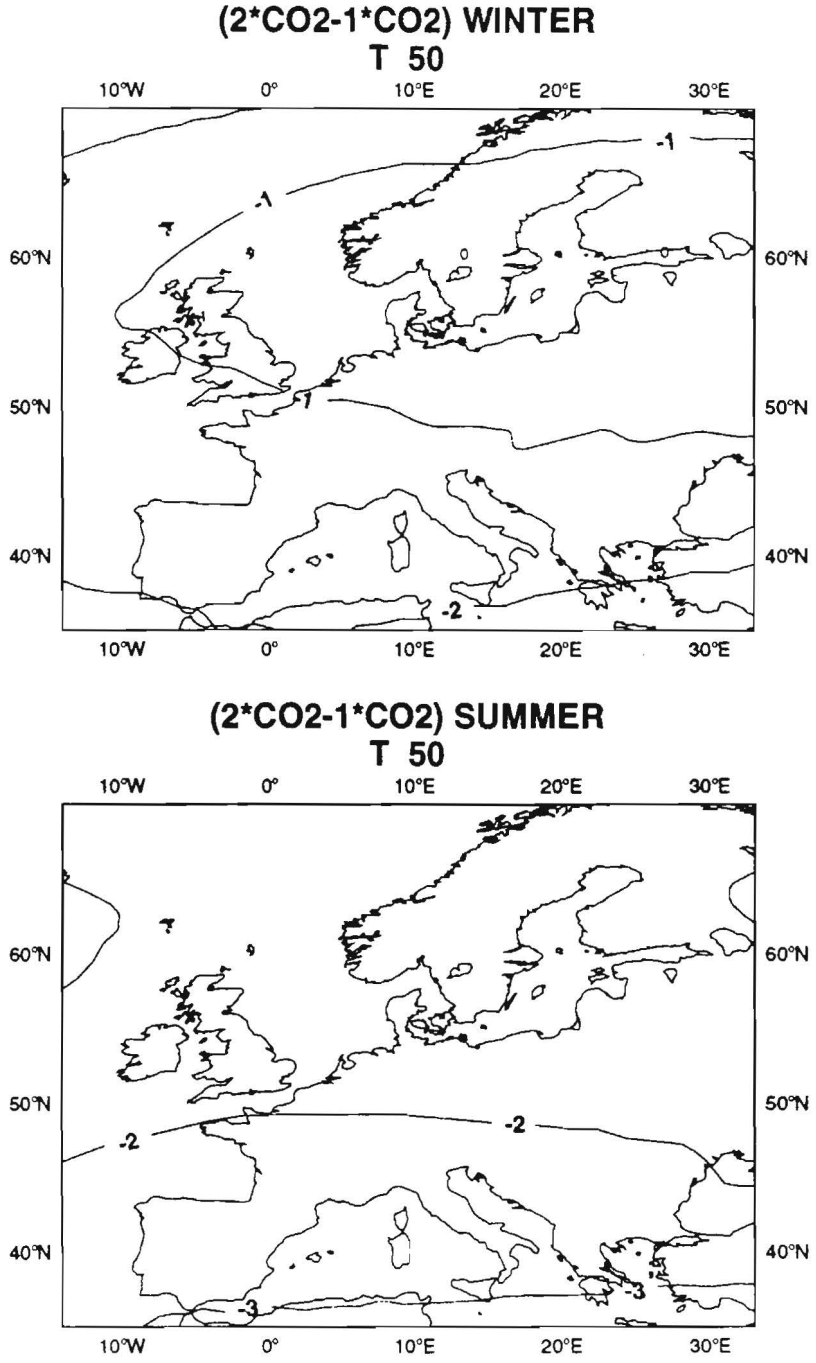

Figure 14: Anomalies of the **50 hPa Temperature** for winter and summer. The contour interval is 1.0°C.

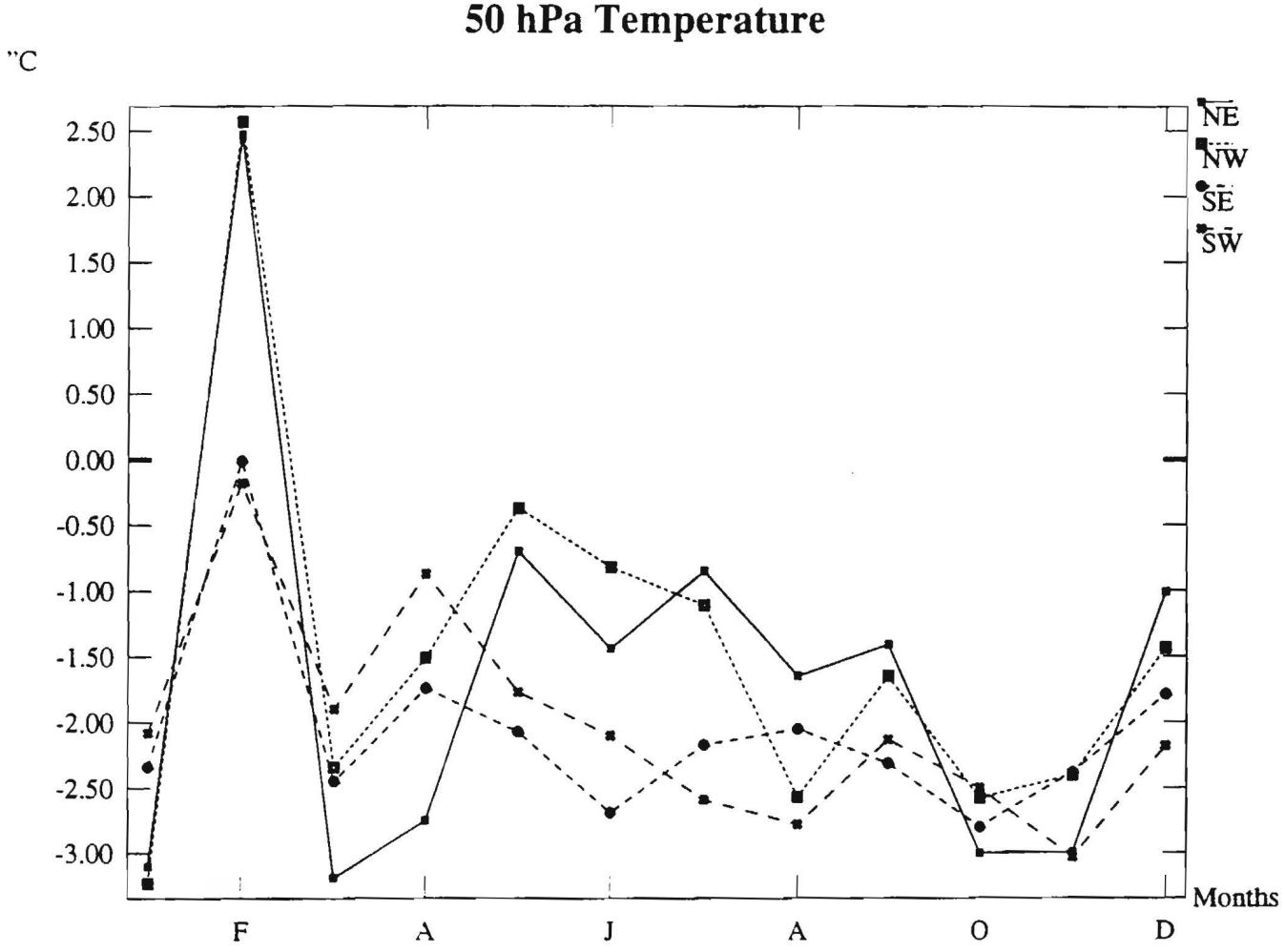

Figure 15: Anomaly monthly mean **50 hPa Temperature** (°C) for the four European subdomains (NW, NE, SW and SE)

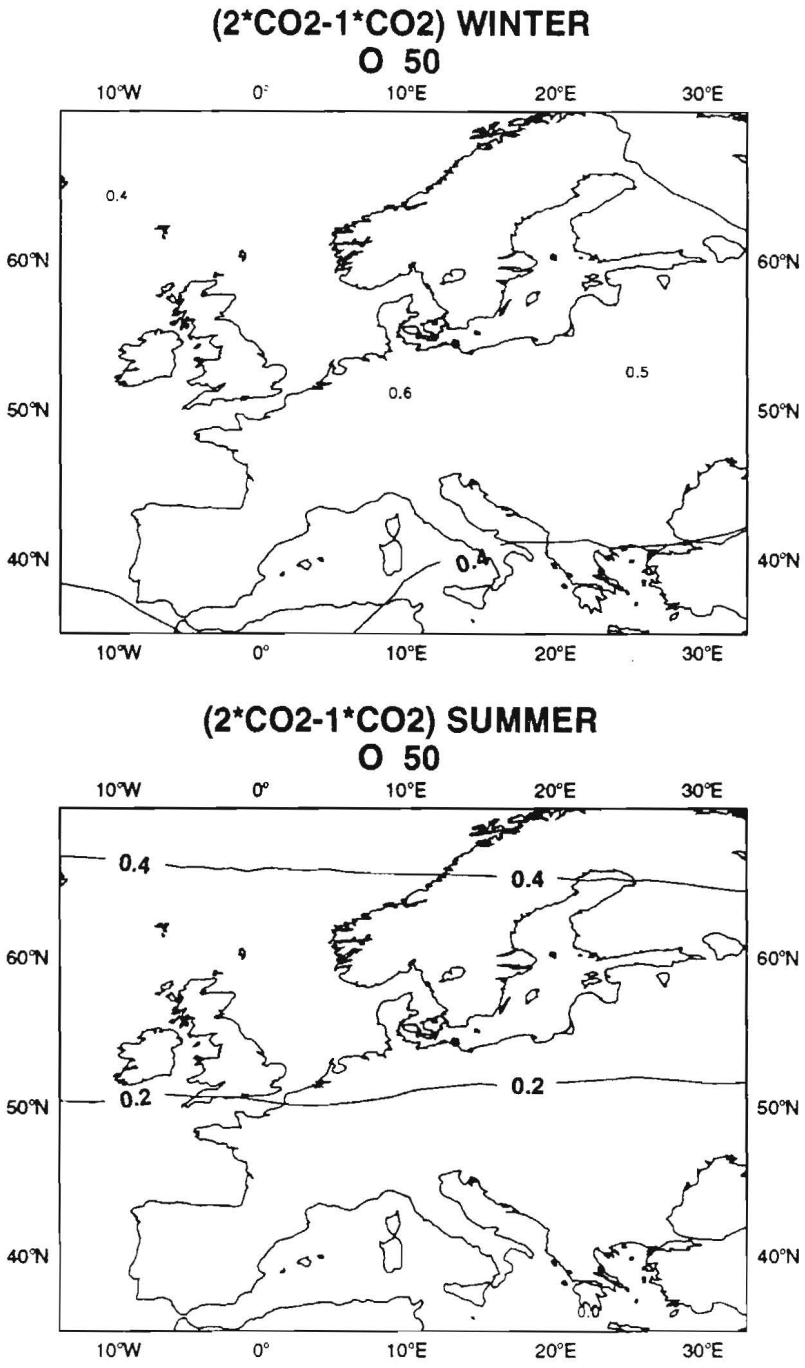

Figure 16: Anomalies of the **50 hPa Ozone** for winter and summer. The contour interval is 0.2 ppm.

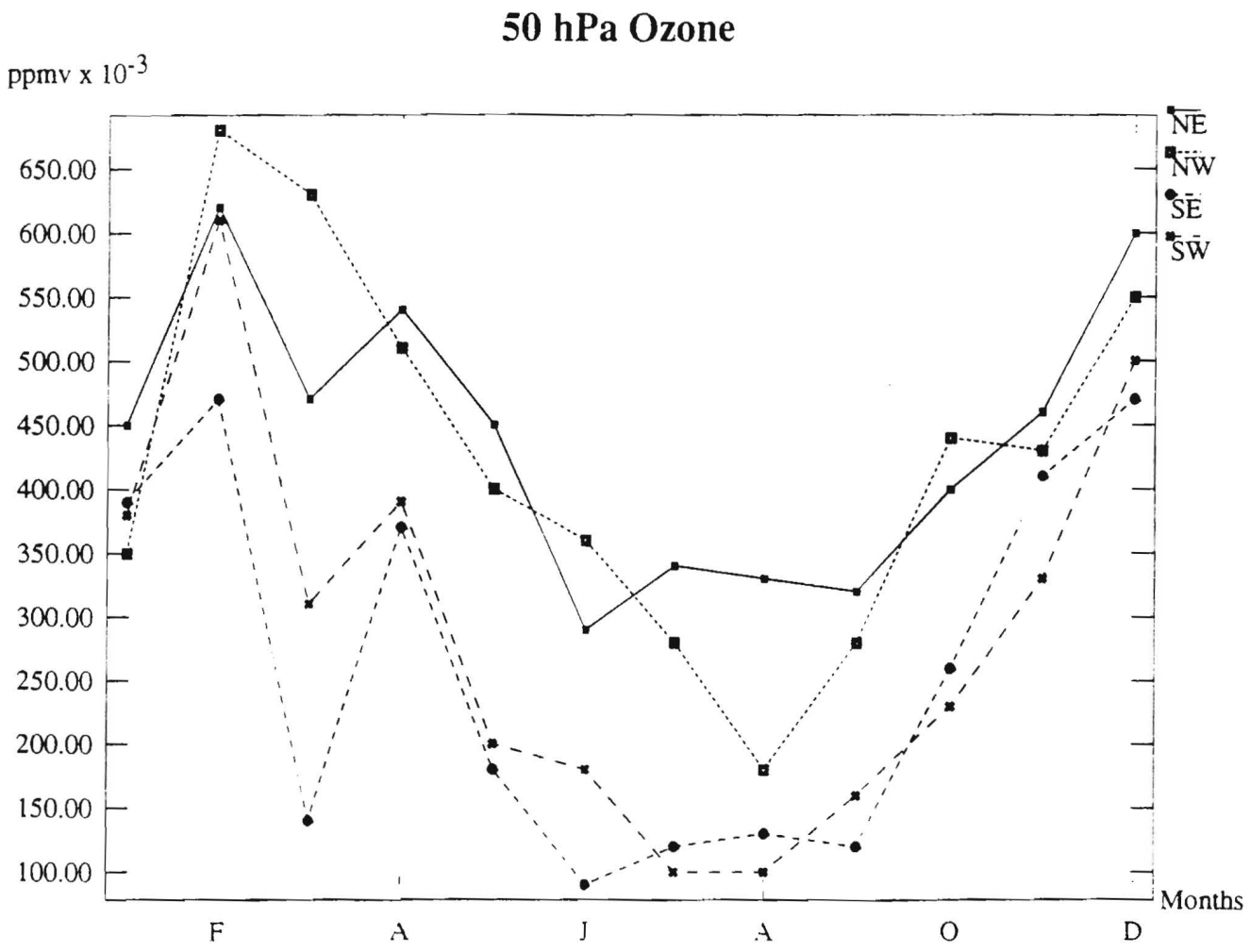

Figure 17: Anomaly monthly mean **50 hPa Ozone** (ppm) for the four European subdomains (NW, NE, SW and SE)

10 List of tables

List of Tables

Variable	NW	NE	SW	SE	EUR
Temperature (2m)(°C)	1.28	1.54	1.80	1.56	1.55
Cloud Rad. Forc.(W/m^2)	-0.84	-1.75	1.09	2.40	0.22
Precipitation (mm/day)	-0.04	0.00	-0.13	-0.27	-0.11
Evaporation (mm/day)	-0.04	0.01	-0.11	-0.21	-0.09
10 hPa Temperature (°C)	-4.84	-4.64	-5.25	-5.32	-5.02
50 hPa Temperature (°C)	-1.46	-1.64	-2.01	-2.07	-1.79
500 hPa Temperature (°C)	1.85	1.71	2.34	2.35	2.06
850 hPa Temperature (°C)	1.37	1.37	1.78	1.50	1.51
10 hPa Ozone (ppmv)	0.57	0.56	0.57	0.58	0.57
50 hPa Ozone (ppmv)	0.43	0.44	0.29	0.26	0.35
Total Ozone (Du)	21.57	22.21	15.76	16.11	18.91

Table 1. Annual-mean anomalies for the four European subdomains (NW, NE, SW and SE) and the full domain (EUR).